AUCTORES
Globalize your Research

New Medical Innovations and Research

Ali Shanaghi * & Ali Reza Souri *

Open Access

Research Article

Electrochemically Deposited Biomimetic Hydroxyapatite-Collagen Coating on Ti6Al4V: Enhancing Corrosion Resistance and Nanomechanical Performance for Medical Applications

Ali Shanaghi *, Alireza Souri *, Seyed Peyman Aiyoubian Markazi, Sajjad Lak

Department of Materials Engineering, Faculty of Engineering, Malayer University, Malayer, Iran.

***Corresponding Authors:** Dr. Ali Shanaghi and Dr. Ali Reza Souri, Department of Materials Engineering, Faculty of Engineering, Malayer University, Malayer, Iran.

Received date: January 18, 2025; **Accepted date:** February 12, 2025; **Published date:** March 10, 2025

Citation: Ali Shanaghi, Alireza Souri, Seyed Peyman Aiyoubian Markazi, Sajjad Lak, (2025), Electrochemically Deposited Biomimetic Hydroxyapatite-Collagen Coating on Ti6Al4V: Enhancing Corrosion Resistance and Nanomechanical Performance for Medical Applications, *J New Medical Innovations and Research*, 6(3); **DOI:**10.31579/2767-7370/139

Abstract:

This study investigated the synergistic effects of incorporating collagen type I into hydroxyapatite (HA) coatings on anodized Ti-6Al-4V substrates to enhance their biocompatibility and performance for biomedical applications. HA coatings were electrochemically deposited onto anodized Ti-6Al-4V, and collagen was subsequently incorporated via a soaking method. The coatings were characterized using GI-XRD, FESEM, AFM, nanoindentation, nanoscratch testing, and EIS. GI-XRD confirmed the presence of both anatase and rutile TiO2 in the anodized layer and revealed that collagen influenced HA crystallization, promoting the formation of aligned, elongated HA crystals. FESEM and AFM analyses showed a 30% reduction in surface roughness upon collagen incorporation, attributed to collagen filling HA pores. Nanoindentation testing demonstrated a decrease in Young's modulus from 0.2 GPa for HA to 0.1 GPa for the HA-collagen composite, and hardness decreased from 0.07 GPa to 0.01 GPa, respectively. Nanoscratch testing revealed improved wear resistance for the HA-collagen composite, with the coefficient of friction decreasing from 1.12 to 0.94 during scratching. EIS studies showed a two-fold increase in charge transfer resistance for the HA-collagen coating, indicating enhanced corrosion protection. These results suggest that the HA-collagen composite coating offers a promising approach for improving the long-term performance and clinical success of biomedical implants by enhancing cell adhesion, mitigating stress shielding, improving wear resistance, and enhancing corrosion protection.

Keywords: electrochemical deposition; hydroxyapatite-collagen; corrosion behavior; nano-mechanical properties; ti6al4v

1.Introduction

Titanium (Ti) and its alloys are widely used as implant materials for replacing damaged load-bearing bones due to their excellent corrosion resistance, high mechanical strength, low density, and good biocompatibility [1]. Despite these advantages, titanium and its alloys face certain challenges when used as implants. Their bioinert nature often hinders bone tissue integration, and they may release undesirable ions, which can lead to adverse biological responses [2]. Additionally, titanium alloys are susceptible to reactions with corrosive ions present in body fluids, which can result in damage to adjacent tissues and structures [1–3]. Other issues, such as severe adhesive wear and stress shielding effects, further limit their performance as long-term implant materials [1–3]. To address these shortcomings, surface modifications, such as the hierarchical deposition of hydroxyapatite-collagen (Col/HA) composites on anodized Ti6Al4V alloys, have been proposed. These modifications aim to enhance biological compatibility and reduce the adverse effects associated with titanium-based implants [4].

Hydroxyapatite (HA), a key mineral component of human bone and teeth, is a calcium phosphate compound with the chemical formula Ca10(PO4)6(OH)2 [5–7]. Due to its excellent biocompatibility and osteoconductivity, HA-based nanocomposites have been extensively used in biomedical applications, including bone repair and regeneration [7–9]. Similarly, type I collagen, which constitutes about 90% of bone tissue, provides structural integrity and support for various connective tissues, including bone, skin, and tendons [10]. Recently, collagen has gained significant attention for its applications in tissue engineering and regenerative medicine [11, 12]. Combining HA with collagen in a nanocomposite coating offers the advantages of both materials, resulting in improved biocompatibility and osteoconductivity, along with the ability to mimic the hierarchical structure of natural bone [12–14].

Various coating techniques are available for producing HA layers on metallic substrates, including sol-gel [15–18], thermal and plasma spraying [19–22], biomimetic processes [23, 24], chemical vapor deposition [25], pulsed laser deposition [26, 27], and electrochemical

deposition [28, 29]. Electrochemical deposition is an effective and versatile method for synthesizing HA coatings on Ti6Al4V alloys. This technique utilizes an applied electric field to deposit HA layers from an electrolyte solution onto the metallic substrate, offering advantages such as simplicity, low cost, and precise control over coating morphology and thickness [46]. Additionally, this method allows the formation of porous coatings, which facilitate bone ingrowth and improve implant fixation [43, 44]. However, the deposition process requires subsequent sintering at elevated temperatures to enhance the mechanical integrity and adhesion of the coatings. This sintering step, particularly at high temperatures exceeding 950 °C, can result in the decomposition of HA into undesirable calcium phosphate phases [50].

To ensure the integrity of nano-composite HA layers, sintering must be conducted at significantly lower temperatures compared to traditional microparticulate counterparts. These nano-composite coatings are derived from stable, non-agglomerated suspensions prepared using nano-sized starting powders. The use of a dispersing agent is critical to prevent particle agglomeration during the synthesis process. However, challenges arise during the sintering process, including the formation of cracks in the HA layer due to mismatched thermal expansion coefficients between the HA coating and the metallic substrate. Furthermore, significant differences in the chemical and structural properties of the materials hinder the formation of a strong chemical bond between the deposited HA layer and the Ti alloy substrate at their interface [50-59].

However, this article introduces a novel approach to enhancing the performance of anodized Ti6Al4V implants by developing a hierarchical collagen-hydroxyapatite (Col/HA) nanocomposite coating, integrating advanced electrochemical and precipitation techniques. The research aims to overcome the limitations of traditional titanium implants, such as bioinertness and ion release, by mimicking the natural structure of bone tissue. The use of collagen, a key component of type I human bone, combined with hydroxyapatite—a primary constituent of bone minerals—results in a biomimetic coating that significantly improves corrosion resistance, mechanical properties, and biocompatibility. By employing optimized deposition techniques, this article demonstrates a novel strategy for achieving strong adhesion between the coating and Ti6Al4V substrate, along with enhanced nanomechanical performance and superior cellular response. This innovative work provides a significant leap toward the design of next-generation medical implants, offering improved durability, bioactivity, and compatibility for dental and orthopedic applications.

2.Experimental

2.1. Substrat preparation

The experimental process commenced with the preparation of samples cut from a Grade 5 titanium sheet, commonly known as Ti-6Al-4V. Each sample was precisely machined to dimensions of 10 mm × 20 mm × 1 mm. To address any surface imperfections resulting from the cutting process, a systematic surface preparation protocol was employed. This involved sequential sanding using sandpaper with grit sizes of 800, 1000, 1500, 2000, 2500, and 3000. Following sanding, the samples were polished using a metallographic cloth in conjunction with an alumina suspension to achieve a high-quality finish. To ensure the removal of contaminants, the polished samples underwent a degreasing step. Each sample was immersed in acetone and then in 96% ethanol for a duration of 10 minutes. After degreasing, the samples were thoroughly rinsed with distilled water and allowed to air dry completely.

The anodization of the Ti6Al4V samples was performed in a sulfuric acid solution with a concentration of 10-15% at a controlled temperature of 25°C. The anodization process was carried out at a low voltage of 20 volts for a duration of 2 hours. This treatment resulted in the formation of a protective oxide layer on the titanium surface, enhancing its corrosion resistance and mechanical properties.

2.2. Coatings preparation

The hydroxyapatite (HA) coating solution was prepared by dissolving specific reagents in 100 mL of distilled water at a controlled temperature of 45°C. The components utilized for the solution preparation included: Calcium nitrate tetrahydrate, Ammonium dihydrogen phosphate and Sodium nitrate. The pH of the solution was carefully adjusted to approximately 4.5 using appropriate buffering agents. Following this adjustment, 1 mL of hydrogen peroxide was added to facilitate the reaction. The resulting solution was then placed in an ultrasonic bath at a temperature of 30°C for one hour to ensure complete homogeneity and uniform particle distribution. Then, the HA coating was applied via an electrochemical deposition process using a two-electrode configuration. In this setup, the titanium substrate served as the cathode while a stainless steel electrode acted as the anode. The substrates were immersed in the hydroxyapatite-titania solution and subjected to an electric potential of 3.1 volts at a temperature of 37°C for a duration of 15 minutes to promote effective coating formation.

Finally, the collagen coating was applied by dip coating method onto the hydroxyapatite-coated surface. Edible collagen powder was sourced from a pharmacy, and a solution was prepared by dissolving 500 mg of collagen in one liter of simulated body fluid (SBF) at room temperature. The HA-coated substrates were immersed in this collagen solution for a period of 24 hours to allow for effective adsorption and interaction between the collagen and HA layers. After immersion, the substrates were removed from the solution and allowed to air dry. This immersion-drying cycle was repeated three times to ensure adequate collagen layer formation. Finally, the coated samples were placed in an oven at a temperature of 80°C for 30 minutes to achieve thorough drying and stabilization of the coatings.

2.3. Coating characterizations

The characterization of HA and HA- collagen nanostructured coatings on anodized Ti6Al4V samples was conducted using a range of analytical techniques to evaluate their phase composition, structural properties, chemical composition, thickness, and surface morphology. Grazing-incidence X-ray diffraction (GI-XRD) was performed with a Philips PW-1730 X-ray diffractometer, utilizing Cu(Kα) radiation to record diffraction patterns from $2\theta = 10°$ to 80° with a step size of 0.02°. Incidence angles of $\alpha = 3°$ were employed. The surface morphology and microstructural features were examined through field emission scanning electron microscopy (FE-SEM), while elemental mapping was performed using energy-dispersive X-ray spectroscopy (EDS). Additionally, atomic force microscopy (AFM, NanoscopeVMulti Mode System, Veeco) was utilized to assess surface roughness and topographical characteristics. To investigate the electrochemical properties of the synthesized samples, a three-electrode cell was used containing a platinum mesh as a counter electrode, a Ag/AgCl as a reference electrode, and the samples as a working electrode. The corrosion behavior of the deposited coatings under different conditions was investigated by Electrochemical impedance spectroscopy (EIS) test using a potentiostat/ galvanostat (Metrohm, Autolab IMP) in SBF solution, which prepared with a specific salt composition [60], for 1 h and 24 h at 37 °C and pH 7.4 with a scan rate of +1 mV/s. In addition, EIS was conducted in the range of 10^{-1} to 10^{5} Hz by applying 10 mV as the amplitude and a frequency of 20 mHz in the sweeping mode. Potentiodynamic polarization was conducted in the range of -250 mV to +250 mV versus the open circuit potential at a scanning rate of 1 $mV.s^{-1}$. The corrosion current (i_{corr}) and potential (E_{corr}) were determined by Tafel extrapolation [61]. The nano-mechanical properties such as Young's modulus (E) and hardness were obtained by nano-indentation and nano-scratch tests on the HysitronTriboScope. The nano-indenters with a spherical diamond tip (radius of 1 μm) made by D.R. U.D. Hangen, SURFACE, Huckelhoven were installed on the NanoScope III AFM. This test was conducted with the load control method, in which the applied load to the indenter was increased gradually up to a predetermined maximum load and then reduced continuously to zero. The load and relevant diamond tip displacement were recorded and the hardness and elastic modulus were determined from the continuous

loading and unloading curves. To improve the statistics, each test was repeated 5 times.

3.Results and discussion

3.1. Phase and structural properties

The GI-XRD patterns of anodized Ti6Al4V, hydroxyapatite (HA) coatings, and HA-collagen composite coatings applied to the anodized Ti6Al4V substrate are presented in Figure. 1. These patterns reveal the intricate interplay of titanium dioxide polymorphs, namely anatase and rutile. This mixed-phase oxide layer is characteristic of titanium anodization processes, which result from the complex interactions of electrochemical reactions and oxide growth dynamics at the titanium-electrolyte interface. The presence of anatase was confirmed by reflections corresponding to the (112), (105), (220), and (215) crystallographic planes, while the rutile phase was identified by its reflections from the (111) and (310) planes. Although the relative intensities of these peaks were not quantified, they qualitatively suggest the distribution of the two phases [53-55].

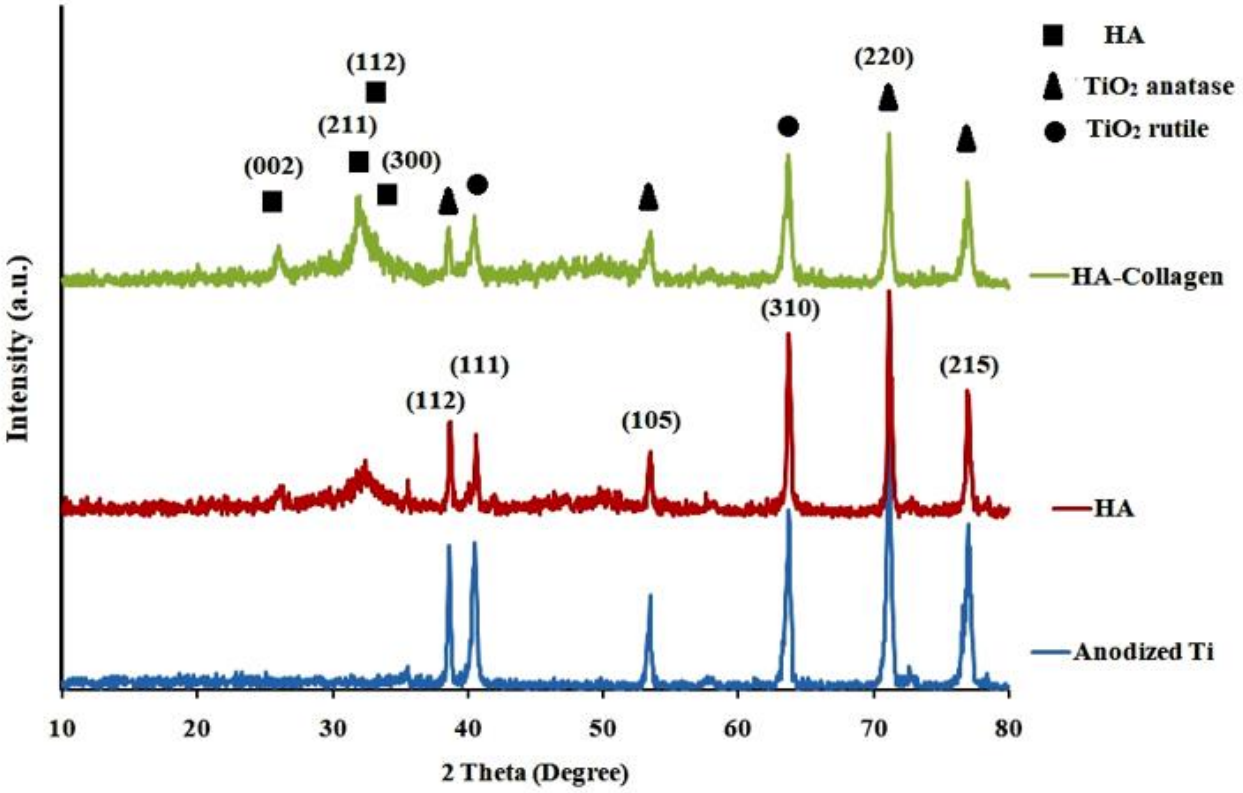

Figure 1: GI-XRD patterns of anodized Ti6Al4V, hydroxyapatite (HA) coatings, and HA-collagen composite coatings applied to the anodized Ti6Al4V.

Notably, the anatase-to-rutile ratio plays a pivotal role in defining the functional attributes of the oxide layer, particularly its photocatalytic behavior and corrosion resistance. The subsequent deposition of the HA coating introduced new reflections into the GI-XRD patterns, corresponding to the (002), (211), (112), and (300) planes of HA. These peaks, consistent with the ICDD PDF card # 00-009-0432, confirm the successful formation of the HA phase on the anodized titanium substrate. Interestingly, the peaks associated with the underlying anatase and rutile phases remained visible, indicating that the HA coating is not entirely dense. This observation suggests that the coating possesses a degree of porosity, allowing X-rays to penetrate through the HA layer and interact with the underlying oxide. Such porosity is often characteristic of HA coatings produced by various deposition techniques and has both beneficial and detrimental implications. While it provides a favorable structure for cell infiltration and osseointegration, it may also compromise the coating's mechanical integrity and corrosion resistance. Furthermore, the incorporation of collagen into the HA coating induced subtle yet significant changes in the GI-XRD patterns. While the characteristic peaks of HA retained their positions, their intensities increased noticeably compared to the HA-only coated sample. Concurrently, the intensities of the anatase and rutile substrate peaks were attenuated. These observations suggest that the HA-collagen composite coating is thicker than its HA-only counterpart. It is plausible that collagen, introduced during the deposition process, acted as a growth promoter for the HA phase by influencing its nucleation and growth kinetics. This effect may arise from collagen's ability to provide nucleation sites or alter the local chemical environment, thereby enhancing crystal growth in SBF solution. magnification applied to the anodized Ti6Al4V substrate.Collagen, being an organic macromolecule, typically does not produce sharp, distinct peaks in XRD patterns. Instead, its presence may manifest as an increase in background noise or a broad, low-intensity feature. While these subtle contributions are challenging to deconvolute without advanced analytical techniques, the overall changes in the XRD patterns provide valuable insights into the structure and composition of the HA-collagen composite coating [53-54].

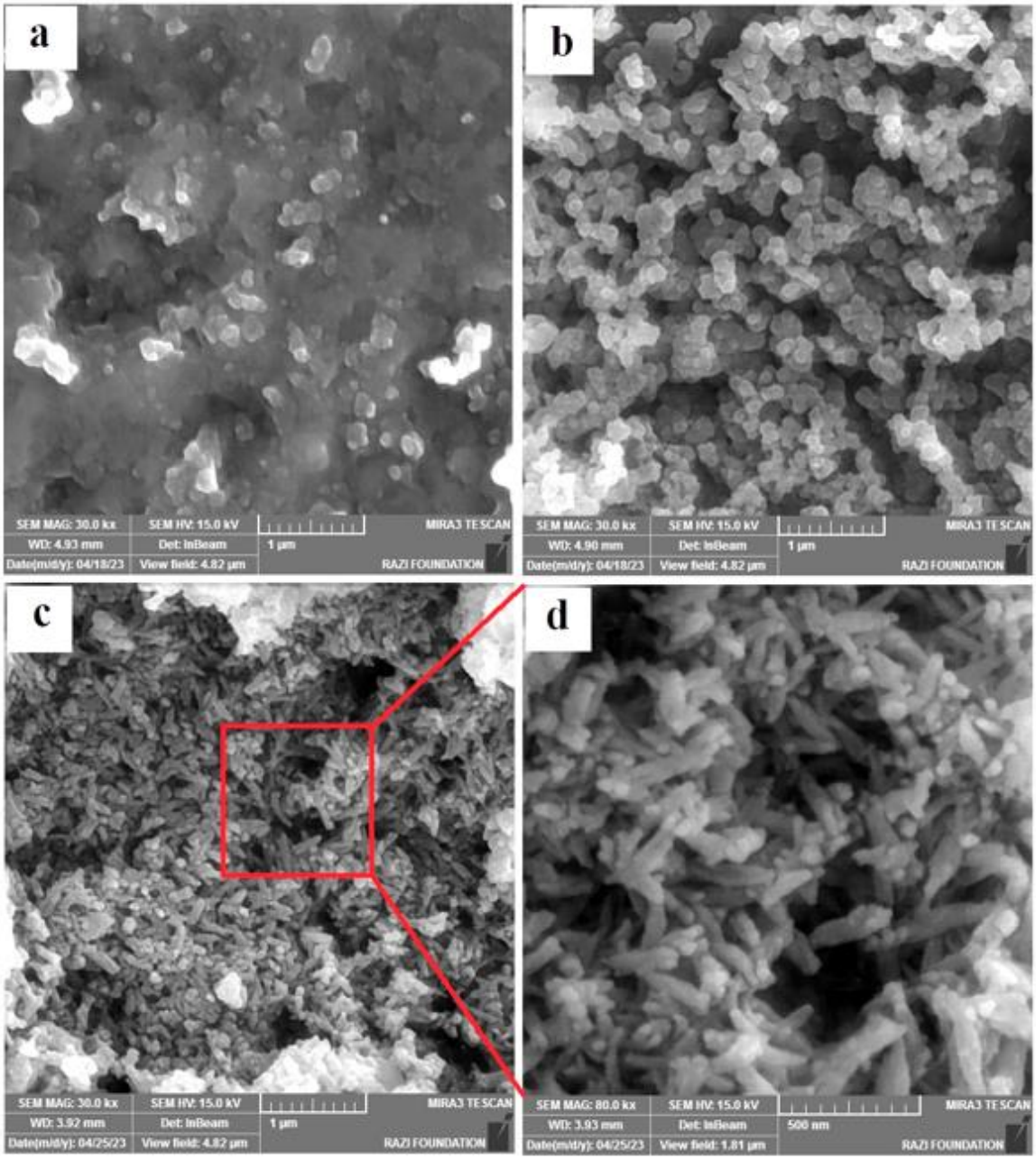

Figure 2. FESEM images of: (a) anodized Ti6Al4V; (b) hydroxyapatite (HA) coating, (c) HA-collagen coating at 30,000× magnification, ; and (d) HA-collagen coatings at 80,000×.

Figures. 2 (a-c) displays FESEM images taken at 30,000x magnification, showcasing anodized Ti6Al4V, hydroxyapatite (HA) coatings, and HA-collagen coatings. These images reveal two main types of HA crystal morphologies: platelet-like and needle-shaped (or rod-like). Notably, in Fig. 2b, numerous spherical HA particles can be seen on the surface of the substrate. This variation in morphology points to a complex interaction of nucleation and growth mechanisms during electrodeposition. Factors such as localized differences in supersaturation, ion concentration gradients near the electrode, and the effects of the anodized layer underneath likely contribute to the observed mixed morphologies. This variety in surface structures is significant because surface roughness and morphology directly impact protein adsorption and subsequent cell attachment. The images also highlight spherical, needle-like, and flower-like (or rosette-like) HA formations [57-59]. Fig. 2c further explores how collagen type I influences the morphology of calcium phosphate (Ca-P) coatings deposited using a sol-gel method. In the absence of collagen, the Ca-P layer appears flat and uniform (as seen in Figs. 2c and 2d). However, when 500 mg/L of collagen type I is introduced into simulated body fluid (SBF) for 24 hours, the morphology changes significantly. The crystallites become smaller and curved, while collagen fibrils become visible within the Ca-P layer. Flake-like Ca-P minerals form on these fibrils, indicating a mineralization process. These mineralized collagen fibrils are tightly integrated into the substrate via the Ca-P crystal network, forming a bilayer structure. This structure creates a biomimetic scaffold that supports implant integration and early cell adhesion and growth. Fig. 2d, at a higher magnification of 80,000x, provides a closer look at the needle-like structures in the HA-collagen coating. These needles are seen as assemblies of smaller spherical particles aligned along a common axis, a pattern strongly influenced by the collagen fibers. The fibers act as templates for HA crystallization, highlighting the organic-inorganic interplay. It's evident that collagen infiltrates the pores of the HA coating after electrodeposition, enhancing the coating's biomechanical and biological properties.

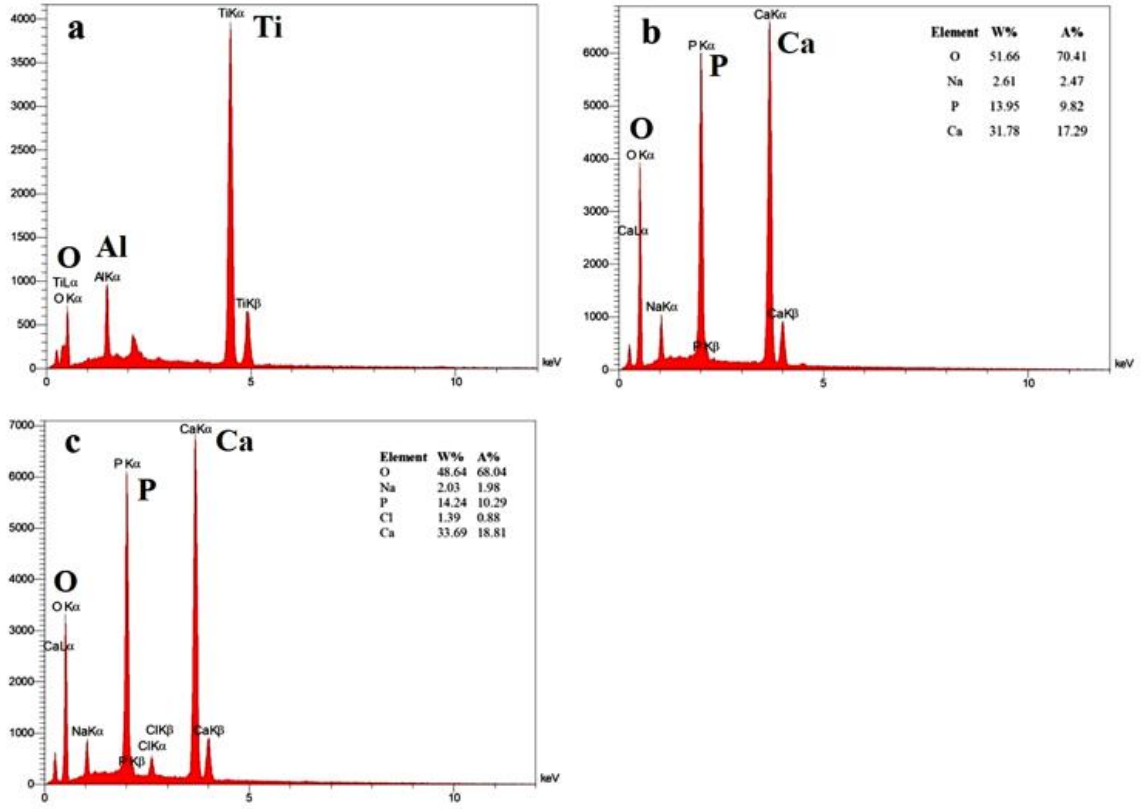

Figure 3: EDS analyses of: (a) anodized Ti6Al4V substrate; (b) hydroxyapatite (HA) coating; and (c) HA-collagen composite coating applied to the anodized Ti6Al4V substrate

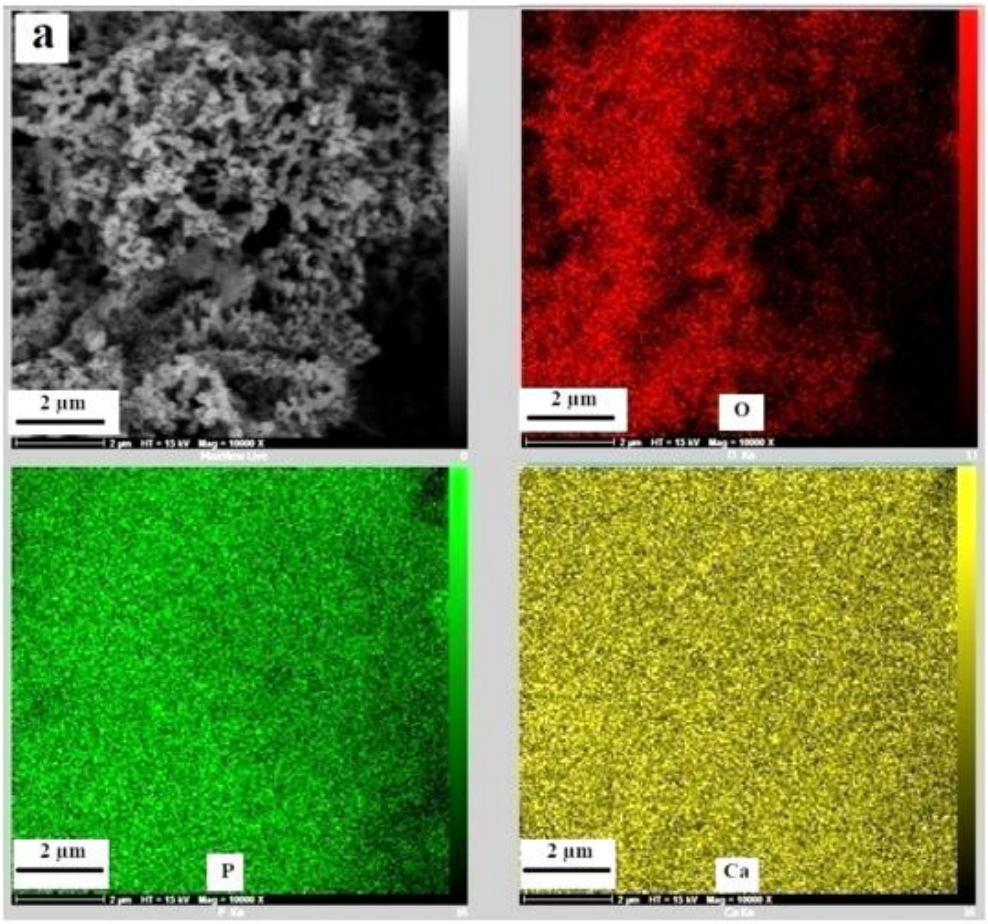

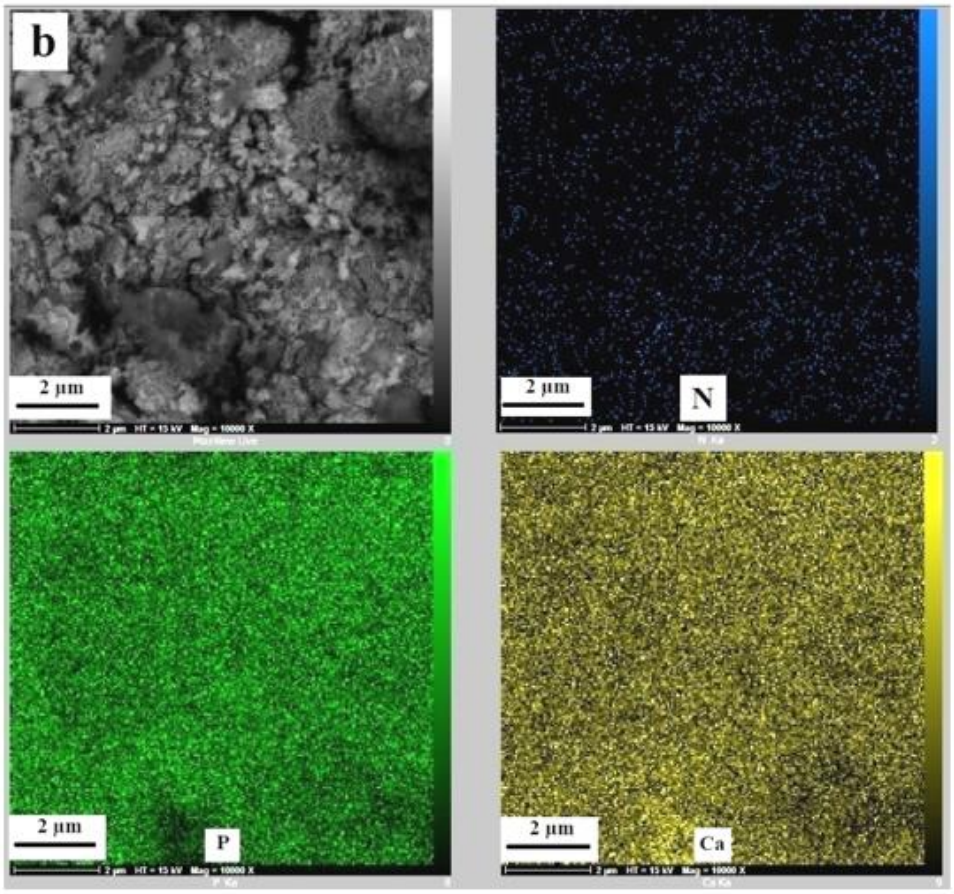

Figure 4: Elemental mapping of: (a) anodized Ti6Al4V substrate; (b) hydroxyapatite (HA) coating; and (c) HA-collagen composite coating applied to the anodized Ti6Al4V substrate.

Energy-dispersive X-ray (EDX) analysis (Figure. 3) determined the Ca/P molar ratio of the HA coating to be 1.76, which is close to the ideal stoichiometric ratio of HA (1.67) [62-63]. Minor deviations could stem from surface contamination, slight compositional variations, or the inherent limitations of the EDX technique, which analyzes a relatively large area. The analysis confirmed the presence of key elements (Ca, P, O, Ti, Al, and V) in all three samples. And also, elemental mapping (Figure. 4) provided further insight into the distribution of elements within the coatings. The maps showed a uniform distribution of calcium, phosphorus, and oxygen in both HA and HA-collagen coatings, indicating a controlled and consistent deposition process. For HA-collagen coatings, the nitrogen map revealed an even distribution of collagen throughout the HA matrix, critical for creating a biomimetic environment that supports uniform cell interactions and predictable tissue regeneration.

By combining data from SEM, EDX, and elemental mapping, a detailed understanding of the coating structure and composition emerges. SEM highlights how collagen affects HA morphology, creating a thicker coating with aligned needle-like structures. EDX confirms the near-stoichiometric HA composition, while elemental mapping underscores the homogenous dispersion of collagen in the composite. These findings demonstrate the potential of HA-collagen coatings to enhance biological and mechanical properties, making them ideal for biomedical applications.

3.2. Thermodynamic Considerations and Reaction Sequence in Hydroxyapatite Coating Electrodeposition

The extent of surface coverage by these deposits is primarily determined by the nucleation and growth ability of the target material from a thermodynamic perspective. Given this information, it is crucial to carefully control the formation mechanism of the hydroxyapatite layer during the electrodeposition process. Hydroxyapatite coatings are produced through a series of reactions that are essential for successful electrodeposition, they are [64-65]:

$$2H_2O + 2e^- \rightarrow H_2 \uparrow + 2OH^- \quad (1)$$

$$H_2PO_4^- + OH^- \rightarrow HPO_4^{2-} + H_2O \quad (2)$$

$$HPO_4^{2-} + OH^- \rightarrow PO_4^{3-} + H_2O \quad (3)$$

$$Ca^{2+} + HPO_4^{2-} + 2H_2O \rightarrow CaHPO_4.2H_2O \downarrow \quad (4)$$

$$5Ca^{2+} + 3PO_4^{3-} + OH^- \rightarrow Ca_5(PO_4)_3(OH) \downarrow \quad (5)$$

$$10CaHPO_4 + 2OH^- \rightarrow Ca_{10}(PO_4)_6(OH)_2 \downarrow + 4PO_4^{3-} + 10H^+ \quad (6)$$

The hydroxyl groups (OH^-) required for HA synthesis are provided from the water electrolysis reaction according to Eg. 1. Increasing the pH values near the cathode surface promotes the $H_2PO_4^-$ (as the stable phosphate salt at pH value 4.5) to react with hydroxyl ions to create $H_2PO_4^{2-}$ (see Eq. 2) [64]. The increase in hydroxyl concentration results in an increase in PO_4^{3-} ions according to Eq. 3. The brushite (dicalcium phosphate dihydrate, DCPD) will be produced as a result of the combination of Ca^{2+} and HPO_4^{2-} ions according to Eq. 4. In addition, hydroxyapatite deposit materials can emerge by the reaction of Ca^{2+}, PO_4^{3-}, and hydroxyl ion used on Eq. 5. While alkali treatment, the brushite deposited transforms to HA according to Eq. 6. It must be mentioned that hydrogen peroxide added to the electrolyte provides a supplementary source for OH^- generation according to Eq. 4. In such a case, the amount of released hydrogen gas at the cathode surface (Eq. 1) will decrease, which can result in the emergence of coatings having better uniformity and higher adhesion. Nevertheless, it has been proclaimed that the rate of

titanium oxidation will increase at the proximity of the H_2O_2 compound, Eq. 7 [65].

$$H_2O_2 + 2e^- \rightarrow 2OH^- \quad (7)$$

Complete surface coverage indicates the great capability of entire surface points to produce sediment from a thermodynamic point of view. It was claimed by Nielsen that the thermodynamic driving force for calcium-phosphate (CaP) precipitation can be measured by Eq. 8 [66]:

$$\Delta G = -RT \ln (IAP/K_{SP})/n \quad (8)$$

Where T represents the absolute temperature, R is the ideal gas constant, and n shows the number of ions in the precipitate compound material. IAP and K_{SP} represent the ion activity and the thermodynamic solubility product, respectively, that can be granted for HA and DCPD by Eqs. (9-12):

$$IAP\ (HA) = (Ca^{2+})^5(PO_4^{3-})^3(OH^-) \quad (9)$$

$$IAP\ (DCPD) = (Ca^{2+})\ (HPO_4^{2-}) \quad (10)$$

$$Log\ K_{SP}\ (HA) = -1.6657 - 0.098215T - 8219.41/T \quad (11)$$

$$Log\ K_{SP}\ (DCPD) = 18.180752 - 0.0420307T - 3649.5701/T \quad (12)$$

In general, it has been taken into account that the precipitation of CaP coatings while electro-deposition mostly relies on the number of hydroxyl ions (see Eq. 2). It has been proved that despite minor variations in the pH values of the bulk solution, the hydroxyl ions concentration will increase considerably around the cathode surface while electro-deposition. In this regard, CaP precipitates are mostly created on or in the vicinity of the Ti6Al4V cathode surface, the local pH values could be a prime dominant factor affecting the creation of calcium phosphate deposits. According to Eqs. 7–9, at higher pH values the HA is the optimal calcium phosphate phase to precipitate from the solution. Based on Faraday's law in electrolysis, minding that the electricity is entirely consumed bywater reduction and hydroxyl ions production, the maximum theoretical concentration of OH^- in the vicinity of the cathode (alayer with the thickness of δ), the surface can be described by Eq. 13 [67]:

$$[OH^-] = It/zFA\delta \quad (13)$$

Where I indicate the electrical current, z indicates the number of transferred electrons, F indicates the Faraday constant, A indicates the surface area, and t represents for the deposition time. In this work, electrodeposition of HA was carried out on different surfaces under similar process parameters (voltage of 3.1 V, deposition time of 15 min, and the same chemical composition of electrolyte). Generally, it could be said that the difference in the concentration of hydroxyl ions in the proximity of the surfaces and as a result the formation of coatings with unique characteristics was exclusively because of the difference in the surface characteristics of the substrate. It is worth mentioning that the oxide layer created on many surfaces of Ti6Al4V alloy will decrease the effective electrical current during the electro-deposition process. With more increase in the thickness of the oxide layer on the surface, the greater the reduction of the hydroxyl concentration according to Eq.13. The lower concentration of hydroxyl ions at the cathode surface will decrease the ability of calcium-phosphate deposits to generate from a thermodynamic point of view. However, it could be observed that the process parameters employed in this work have resulted in almost the entire coverage of the sample surface. Whereas the HAP electrodeposition at V = 3.1 V and deposition time of 15 min on beta-annealed sample resulted in insufficient surface coverage, as can be seen in Fig. 2b.

The Ca/P molar ratios for synthesized coatings were almost the same as that of HA indicating the presence of sufficient amounts of hydroxyl anions to create hydroxyapatite, based on Eqs. 1-6. Considering that along with almost the entire coverage of the surface by deposits, it can be confirmed that the deposition voltage employed in this work was enough to compensate for the effective current reduction because of the presence of an oxide layer, and as a result, by creating enough amount of hydroxyl ions the coatings would assumingly comprise hydroxyapatite as the prime compound. It can be concluded that the Ca/P molar ratios for calcium phosphate compounds (excluding HA) may have emerged while the electrodeposition process changed from 0.5 for calcium dihydrogen orthophosphate ($Ca(HPO_4)_2$) to 1.5 for three calcium phosphate ($Ca_3(PO_4)_2$) [62-63]. As a result, the presence of such compounds in the structure of the coating layer causes the deviation of the Ca/P ratio from the Ca/P molar ratio of HAP (i.e. 1.76). Taking into account, the Ca/P ratio of the coatings formed in this work could indicate the creation of a higher amount of hydroxyapatite compared to other calcium phosphate compounds during the electro-deposition process.

However, the nucleation and growth mechanism of Ca-P coatings on Ti substrate change while deposition and cause various morphologies at different stages of deposition. Studies [62-67], showed that at the first stage of deposition (t = 1 min), the electrolyte is highly supersaturated and the deposited coatings are polycrystalline HA. The morphology of the coatings at this stage is randomly oriented and highly branched nanoplates. At the second stage (t = 3 min), crystal growth progresses along the b- and c-axes and forms micro-sized plates. At the third stage of deposition, the degree of supersaturation is reduced (t > 10 min), and the deposited crystals propagate along the c-axis and become plate-like or needle-like crystals. According to the above and the electrodeposition time employed in this work (i.e. 15 min), the length of the largest dimension of the plate-likes and needle-likedeposits was assumed as a measure of HAP deposit sizes.

Indeed, plate-like and needle-like HAP crystals in the microstructure (Figure. 2b, 2c and 2d) show that the nucleation and growth of HA crystals are entirely performed on different surfaces. After the nucleation stage, HA will initially generate with spherical crystals. As the deposition time increases, spherical HA crystals will agglomerate to create plate-like crystals. Needle-like morphology is created due to the growth of HA crystals outwards of the plate-like crystals [68- 69].

3.3. Nanomechanical Characterization

Fig. 5 presents AFM images, capturing the surface morphology of the synthesized HA coating and HA- Collagen nanostructured coating deposited on the anodized Ti-6Al-4V substrate within a 5×5 μm² area. These images offer valuable insights into the surface roughness and the arrangement of collagen fibers within the composite structure. The presence of collagen fibers on the surface is evident, with a predominantly parallel orientation. However, discerning individual fibers proves challenging due to the partial obscuring of inter-fiber boundaries. This observation suggests a close packing or intertwining of the collagen fibrils, creating a relatively smooth surface texture at this scale. Actually, comparing the AFM images of the HA and HA-collagen coatings (Figs. 5a- 5b), a noticeable reduction in surface roughness is observed upon collagen incorporation. This reduction suggests that collagen effectively fills some of the pores and irregularities present in the HA structure, leading to a smoother surface finish. This smoothing effect can have profound implications for cell-surface interactions, potentially enhancing cell adhesion, spreading, and proliferation. Furthermore, the presence of collagen can impart a degree of flexibility and resilience to the coating, potentially influencing its mechanical behavior.

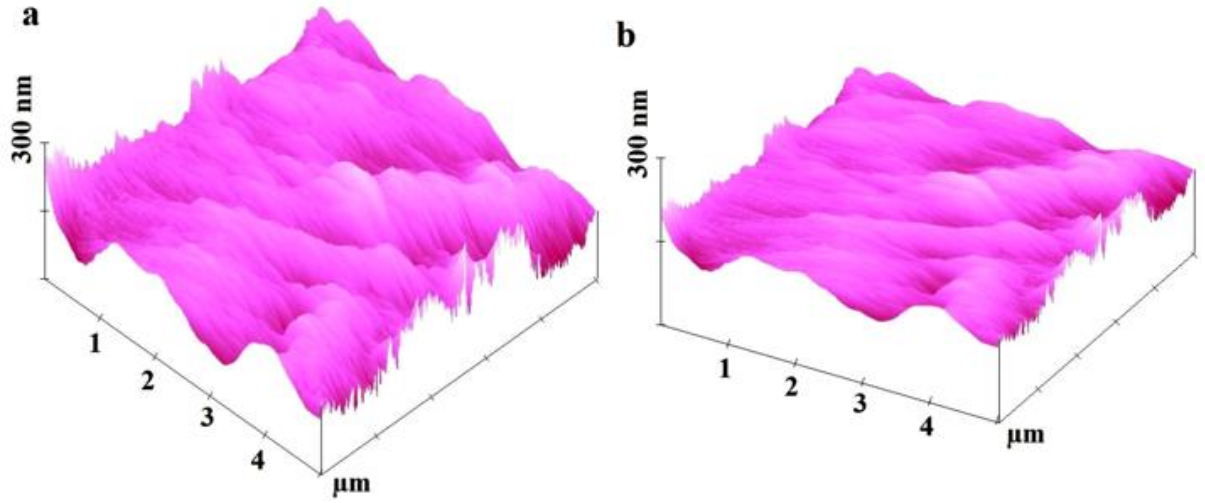

Figure 5: AFM image of: (a) hydroxyapatite (HA) coating; and (b) HA-collagen coating applied to the anodized Ti6Al4V substrate.

The nanomechanical properties of the coatings were investigated using nanoindentation and nanoscratch techniques, performed with an AFM-based nanoindenter. The nanoindentation results, presented in Fig. 6 and summarized in Table 1, reveal a clear trend in both hardness and Young's modulus. As seen in Table 1, both hardness (H) and Young's modulus (E) exhibit a decreasing trend from the anodized Ti substrate to the HA coating and further to the HA-collagen nanostructured coating. Specifically, the Young's modulus decreases from 0.4 GPa for anodized Ti to 0.2 GPa for the HA coating and subsequently to 0.1 GPa for the HA-collagen composite. A similar trend is observed for hardness, decreasing from 0.18 GPa for anodized Ti to 0.07 GPa for the HA coating and finally to 0.01 GPa for the HA-collagen composite. This reduction in both hardness and modulus with the incorporation of HA and, more significantly, with the addition of collagen, is not entirely unexpected. HA, while inherently hard, can exhibit reduced mechanical properties in coatings due to its often porous microstructure. The introduction of collagen, a soft and flexible biopolymer, further reduces the overall stiffness and hardness of the composite material. This decrease in stiffness and hardness can be advantageous in certain biomedical applications, particularly for bone implants, as it can bring the mechanical properties of the coating closer to that of natural bone, mitigating stress shielding effects.

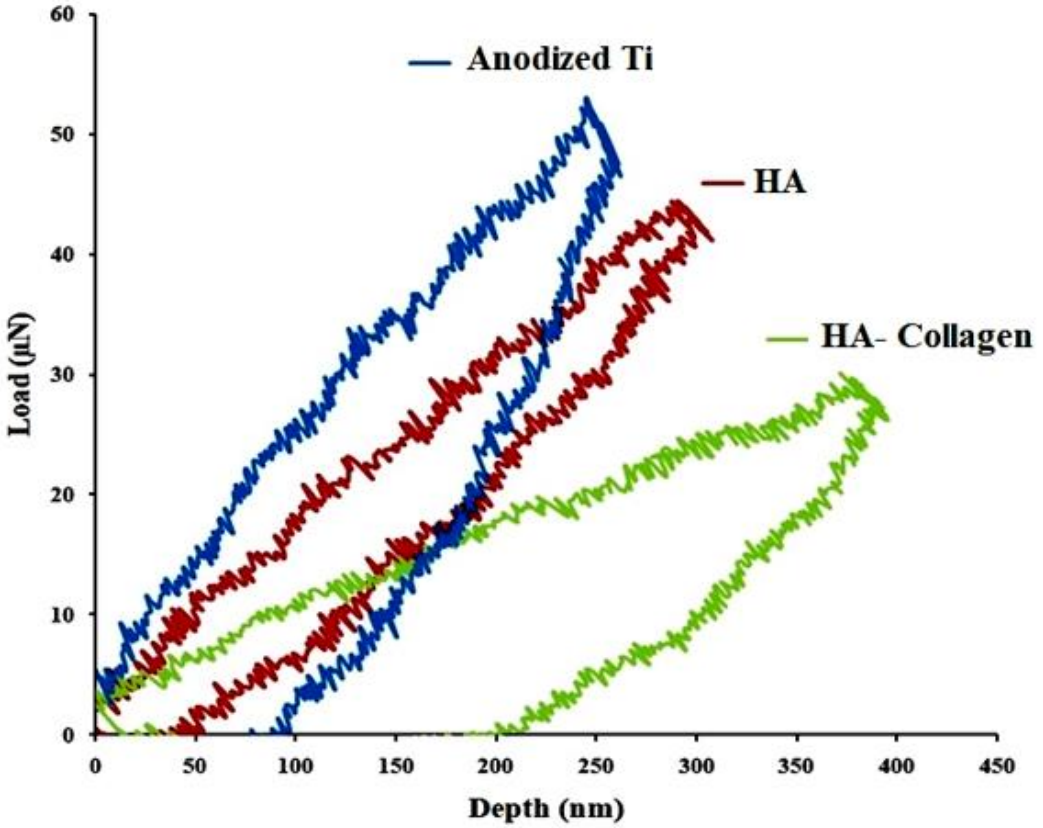

Figure 6: Nano-indentation test of: (a) anodized Ti6Al4V substrate; (b) hydroxyapatite (HA) coating; and (c) HA-collagen composite coating applied to the anodized Ti6Al4V substrate.

Material	Young's modulus (Gpa)	Hardness (Gpa)	Max Depth (nm)	Max Force (µN)
Anodized Ti	0.4	0.18	259	53
HA	0.2	0.07	307	42
HA-Collagen	0.1	0.01	395	28

Table 1: Nanoindentation test data for anodized Ti6Al4V, hydroxyapatite (HA) coating and HA-Collagen nanostructured coating applied on anodized Ti6Al4V

And also, the tribological behavior of the coatings was assessed using nanoscratch testing, the results of which are depicted in Figure. 7. The coefficient of friction (COF) for the anodized titanium shows an increase from an initial value of 0.61 to 0.92 as the scratch test progresses. A similar trend is observed for the HA coating, with the COF increasing from 0.62 to 0.98. This increase in COF during scratching is likely due to wear mechanisms, such as ploughing and micro-cutting, leading to increased surface roughness and frictional resistance. However, the HA-collagen composite exhibits a distinct behavior. The initial COF is higher (1.12), but it *decreases to* 0.94 as the scratch test proceeds. This initial higher COF could be a consequence of the presence of the relatively soft collagen on the surface, which might initially deform more readily under the indenter

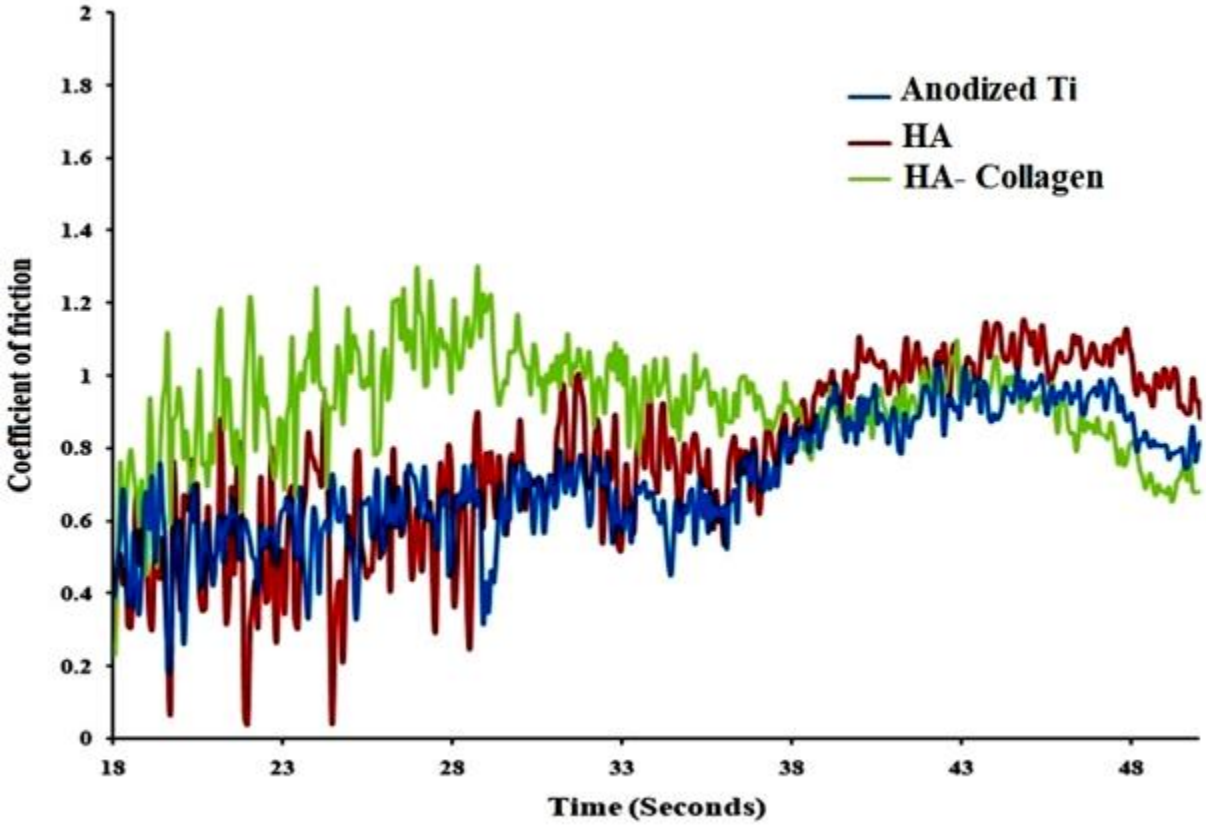

Figure 7: Evolution of the coefficient of friction over time during nano scratch testing of: anodized Ti6Al4V substrate; (b) hydroxyapatite (HA) coating; and (c) HA-collagen composite coating applied to the anodized Ti6Al4V substrate. Test conditions: sliding speed of 1 m/s and applied pressure of 3.45 MPa.

The subsequent decrease in COF suggests that the collagen may be acting as a lubricant, reducing the friction between the indenter and the coating surface. Furthermore, the fibrous nature of collagen could enhance the coating's resistance to ploughing and material removal, preventing a sharp increase in COF typically observed in brittle materials.

The combined analysis of AFM, nanoindentation, and nanoscratch testing provides a holistic understanding of the coating's structure, mechanical properties, and tribological performance. The AFM observations reveal that collagen fills pores in the HA layer, reducing surface roughness. Nanoindentation demonstrates that the incorporation of HA and, especially, collagen reduces both hardness and Young's modulus, a desirable trait for bone implant applications. Nanoscratch testing suggests that collagen can reduce the COF and potentially improve wear resistance. These interconnected findings suggest that combining HA with collagen creates biomimetic coatings with enhanced properties for biomedical applications. Specifically, the reduction in roughness, the tuning of mechanical properties closer to bone, and the improved tribological behavior can collectively contribute to better cell adhesion, reduced implant wear, and improved biocompatibility.

3.4. Corrosion behavior and its mechanism

The nyquist plots and extracted data acquired for different coated surfaces in 1 h and 24h SBF immersion periods are shown in Fig. 8. The corresponding equivalent circuit for the EIS results is depicted in Table 2 in which R_s, R_p, and R_{ct} are solution resistance, the resistance of the coating, which are directly linked to the coating defects such as porosity and microcracks, and charge transfer resistance of electrical double layer

(EDL), respectively. CPE_c and $CPEd_l$ are constant phase elements for coating and EDL, respectively. The fitting curves (solid lines) of the EIS spectra are incorporated into experimental data (scatter points), which are well consistent with each other.

Referring to the fitting results of EIS (Table. 2), the charge transfer resistances of different surfaces (R_{ct}) have a much higher value compared to the corresponding coating resistance (Rc). This is a rather interesting finding. It suggests that, despite the beneficial effects of the HA coating and, even more so, the HA-collagen composite, the overall corrosion resistance of each surface is primarily governed by the charge transfer resistance at the substrate-oxide interface. In other words, the inherent protective properties of the naturally formed or anodically grown oxide layer on the Ti6Al4V substrate play a dominant role in determining the corrosion rate. The coatings, while offering additional protection, primarily influence the impedance behavior at higher frequencies, related to their own dielectric and barrier properties. The anodized Ti6Al4V has the lowest R_{ct} value of 0.89 $M\Omega.cm^2$, which implies a higher corrosion rate than coated samples. The highest R_{ct} value belongs to HA-Collagen nanostructured coating, which means a lower corrosion rate in SBF solution, suggesting that the incorporation of collagen within the HA coating provides a synergistic effect, further enhancing the corrosion protection. This could be attributed to several factors, including a reduction in coating porosity (as observed in the Figure. 2 and Figure. 5), improved barrier properties due to the presence of the organic collagen network, and a possible influence on the electrochemical processes at the interface

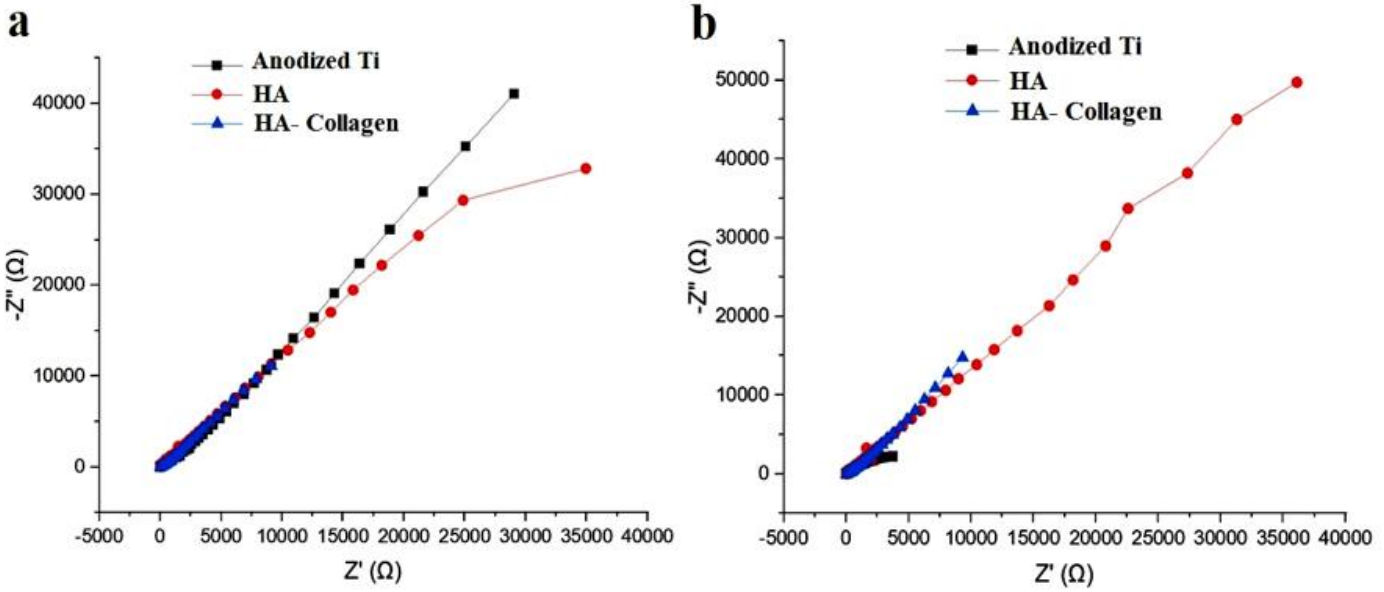

Figure 8: The nyquist plot for anodized Ti-6Al-4V, HA coating, and HA- Collagen nanostructured coating after, a) 1 hour and, b) 24 hours times immersion in SBF solution at 37.5±1.5˚C.

Sample	R_s ($\Omega.cm^2$)	Q_c ($S.sec^n/cm^2$)	nc	R_c ($\Omega.cm^2$)	Qdl ($S.sec^n/cm^2$)	n2	R_{ct} ($\Omega.cm^2$)	W ($S.sec^{0.5}/cm^2$)	R_t ($\Omega.cm^2$)
Ti6Al4V (1h)	0.016	-	-	-	2.25E-5	0.67	0.89	8.37E-5	0.89
Ti6Al4V-HA (1h)	0.03	2.32E-5	0.79	0.04	2.56E-6	0.70	1.96	1.56E-5	1.99
Ti6Al4V-HA-C (1h)	0.021	7.44E-6	0.60	0.22	6.64E-5	0.67	5.48	5.15E-5	5.70
Ti6Al4V (24h)	0.025	8.74E-4	0.65	0.06	7.23E-4	0.64	0.72	-	0.78
Ti6Al4V-HA (24h)	0.024	3.96E-6	0.62	0.31	5.55E-5	0.69	4.97	3.22E-5	5.28
Ti6Al4V-HA-C (24h)	0.01	2.24E-6	0.81	0.68	6.36E-4	0.72	52.89	4.54E-5	53.57

Table 2: EIS data of anodized Ti-6Al-4V, HA coating, and HA- Collagen nanostructured coating after 1 hour and 24 hours times immersion in SBF solution at 37.5±1.5˚C.

Comparatively, the HA- Collagen nanostructured coating has excellent corrosion resistance (Table 2 and Fig.8b) for 24 h immersion in SBF solution compared to its counterparts. As a result, the HA- Collagen nanostructured coating has the highest protective efficiency and in turn outstanding biocompatibility because of the electrochemically deposited HA and particularly sol-gel derived collagen layer on top. These results are in complete agreement with corrosion current densities obtained from polarization curves in Fig. 9, which shows the electrochemical polarization plots for the anodized Ti6Al4V, HA coating and HA-Collagen nanostructured coating, and the results summarized in Table 3. Results indicate that the corrosion rate of anodized Ti6Al4V decreases considerably unlike the sample having optimum coating HA-Collagen layers on its surface. The extremely low corrosion rate is critical in implant applications since it results in the negligible release of toxic metallic ions to the surrounding tissues [17-19].

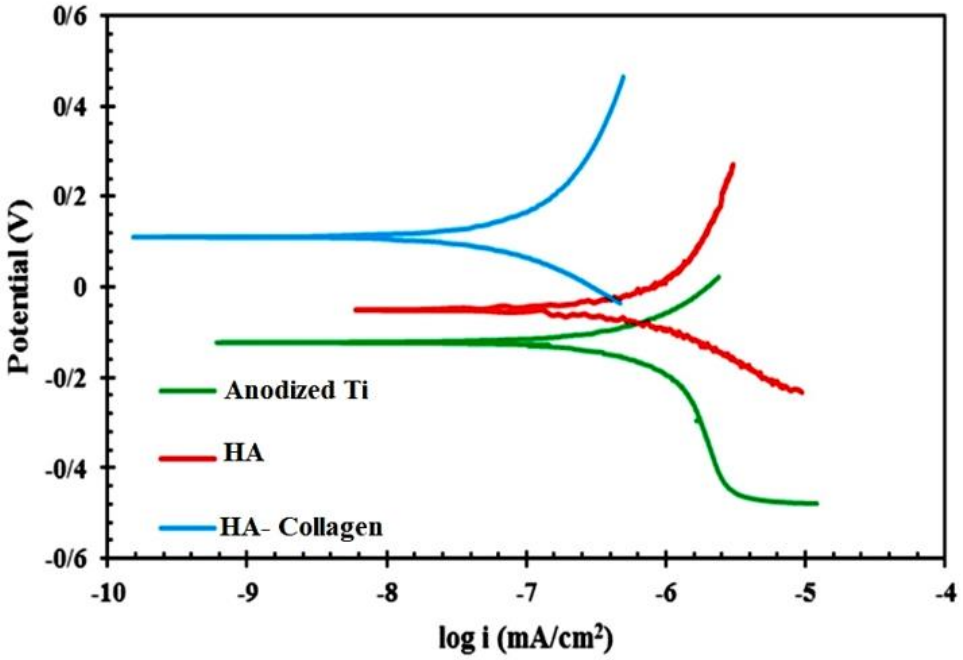

Figure 9: Polarization plot for anodized Ti-6Al-4V, HA coating, and HA-Collagen nanostructured coating in SBF solution at 37.5±1.5˚C.

Samples	β_a (v.dec^{-1})	$-\beta_c$ (v.dec^{-1})	E_{corr} (Ag/AgCl) (V)	i_{corr} (µA/cm^2)	R_p (kohm.cm^2)
Anodized Ti6Al4V	0.189	0.2972	-0.122	0.52	96.5
HA	0.4355	0.169	-0.049	0.447	118.3
HA-Collagen	0.2698	0.177	0.11	0.071	653.6

Table 3: Summarized data of polarization test of anodized Ti-6Al-4V, HA coating, and HA-Collagen nanostructured coating in SBF solution at 37.5±1.5˚C.

Polarization resistance (Rp) values are calculated according to the Eq. (14) [67], and show in Fig. 10:

$$R_p = (\beta_a \times \beta_c) / (2.303 \times i_{corr} \times (\beta_a + \beta_c)) \quad (14)$$

where, i_{corrr} indicates the corrosion current density, β_a and β_c are the anodic and cathodic Tafel constants, respectively, and results show a significant increase in the polarization resistance of the coating containing HA and collagen, so that the polarization resistance has increased by more than 600% compared to anodized titanium and also HA coating. Finally, the observed enhancement in corrosion resistance with the HA-collagen coating suggests its potential for improving the long-term performance and biocompatibility of Ti6Al4V implants.

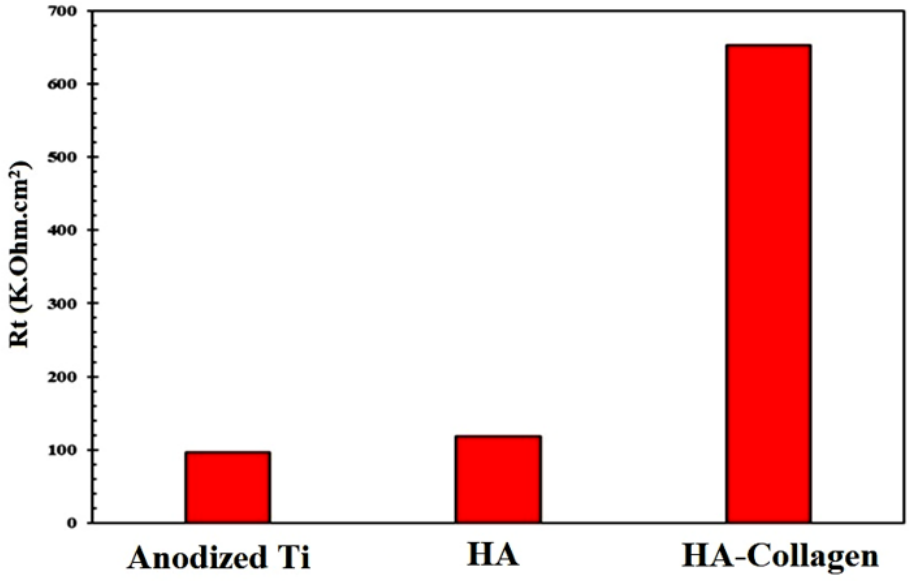

Figure 10: Polarization resistance (R_p) values for anodized Ti-6Al-4V, HA coating, and HA-Collagen nanostructured coating.

Conclusion

This study meticulously investigated the synergistic effects of combining hydroxyapatite (HA) with collagen on anodized Ti-6Al-4V, exploring the resulting coatings' structural, mechanical, tribological, and corrosion properties. GI-XRD analysis confirms the successful development of a multi-layered coating on Ti6Al4V, comprising an anodized titanium layer with mixed anatase-rutile structure, followed by a crystalline HA coating. The addition of collagen enhances HA peak intensities, indicating a thicker, more integrated composite layer. Nanoindentation tests reveal decreasing hardness and Young's modulus from anodized Ti to HA, and further to HA-collagen coatings. This softening, mainly due to collagen addition, potentially benefits bone implants by mimicking natural bone properties. Nanoscratch tests show increasing coefficient of friction (COF) for anodized Ti and HA coatings during scratching, likely due to wear mechanisms. Interestingly, the HA-collagen composite exhibits a unique behavior with an initially higher COF that decreases during testing, suggesting improved tribological properties. EIS and polarization tests reveal that the HA-Collagen nanostructured coating significantly enhances Ti6Al4V implant corrosion resistance in SBF. This composite coating shows a 600% increase in polarization resistance compared to anodized titanium and HA coating alone, exhibiting the highest charge transfer resistance (0.89 $M\Omega.cm^2$) and lowest corrosion rate. The observed reduction in roughness, the tailored mechanical properties, the improved wear resistance, and the enhanced corrosion protection collectively contribute to a more biocompatible and durable coating. These findings strongly suggest that the HA-collagen composite holds considerable promise for enhancing the long-term performance and clinical success of biomedical implants, particularly in orthopedic and dental applications.

Acknowledgements

The work was financially supported by Malayer University Research Grant, No. 1400.

References

1. K. Pałka, R. (2018). Pokrowiecki, Porous titanium implants: a review. Adv. Eng. Mater. 20(5),1–18
2. A. Chandra et al. (2011). Life expectancy of modular Ti6Al4V hip implants: influence of stress and environment. J. Mech. Behav. Biomed. Mater. 4(8), 1990-2001
3. S. Noumbissi, A. Scarano, S. (2019). Gupta, A literature review study on atomic ions dissolution of titanium and its alloys in implant dentistry. Materials (Basel) 12(3), 1-15
4. R.B. Heimann, H.D. (2015). Lehmann, *Bioceramic Coatings for Medical Implants: Trends and Techniques*
5. Bernache-Assollant, D., et al. (2003). Sintering of calcium phosphate hydroxyapatite $Ca_{10}(PO_4)_6(OH)_2$I. Calcination and particle growth. Journal of the European Ceramic Society, 23(2): p. 229-241.
6. Wagh, A., (2016). Chemically bonded phosphate ceramics: twenty-first-century materials with diverse applications.
7. Aaddouz, M., et al. (2023). Removal of methylene blue from aqueous solution by adsorption onto hydroxyapatite nanoparticles. Journal of Molecular Structure, 1288: p. 135807.
8. Chen, F. and Y.-J. Zhu. (2014). Multifunctional calcium phosphate nanostructured materials and biomedical applications. Current Nanoscience, 10(4): p. 465-485.
9. Suchanek, W. and M. (1998). Yoshimura, Processing and properties of hydroxyapatite-based biomaterials for use as hard tissue replacement implants. Journal of materials research, 13(1): p. 94-117.
10. Avila Rodríguez, M.I., L.G. (2018). Rodríguez Barroso, and M.L. Sánchez, Collagen: A review on its sources and potential cosmetic applications. Journal of cosmetic dermatology, 17(1): p. 20-26.
11. Buckley, M. (2016). Species identification of bovine, ovine and porcine type 1 collagen; comparing peptide mass finger printing and LC-based proteomics methods. International journal of molecular sciences, 17(4):p. 445.
12. Henriksen, K. and M. (2016). Karsdal, Type I collagen, in Biochemistry of collagens, laminins and elastin. Elsevier. p.1-11.
13. F. Giovanniello, M. Asgari, I. D. Breslavsky, G. Franchini, G. A. Holzapfel, M. Tabrizian, M. Amabili. (2023). "Development and mechanical characterization of decellularized scaffolds for an active aortic graft". Acta Biomaterialia, 160 59-72.
14. Mushtaq, A., et al. (2021). Magnetic hydroxyapatite nanocomposites: The advances from synthesis to biomedical applications. Materials & Design, 197: p. 109269.
15. P. Choudhury, D.C. (2011). Agrawal; "Sol–gel derived hydroxyapatite coatings on titanium substrates"; Surf. Coat. Tech; 206 360-365.
16. C. Domínguez-Trujillo, E. Peón, E. Chicardi, H. Pérez, Y. (2011). Torres; "Sol-gel deposition of hydroxyapatite coatings on porous titanium for biomedical applications"; Surf. Coat. Tech; 333 158-162.
17. Kazemi, Maryam & Ahangarani, Sh & Esmailian, Mohammad & Shanaghi, Ali. (2022). Investigating the corrosion performance of Ti-6Al-4V biomaterial alloy with hydroxyapatite coating by artificial neural network. Materials Science and Engineering: B. 278. 115644.
18. Shanaghi, Ali &Mehrjou, Babak&Ahmadian, Zahra & Souri, Alireza & Chu, Paul. (2021). Enhanced corrosion resistance, antibacterial properties, and biocompatibility by hierarchical hydroxyapatite/ciprofloxacin-calcium phosphate coating on nitridedNiTi alloy. Materials Science and Engineering C. 118. 1-16.
19. Kazemi, Maryam & Ahangarani, Sh & Esmailian, Mohammad & Shanaghi, Ali. (2020). Investigation on the corrosion behavior and biocompatibility of Ti-6Al-4V implant coated with HA/TiN dual layer for medical applications. Surface and Coatings Technology. 397. 126044.
20. R. T. Candidato, P. Sokołowski, L. Pawłowski, G. Lecomte-Nana, C. (2017). Constantinescu, A. Denoirjean; "Development of hydroxyapatite coatings by solution precursor plasma spray process and their microstructural characterization"; Surf. Coat. Tech; 318 39-49.
21. T. P. Ntsoane, M. Topic, M. Härting, R. B. (2016). Heimann, Ch. Theron; "Spatial and depth-resolved studies of air plasma-sprayed hydroxyapatite coatings by means of diffraction techniques: Part I"; Surf. Coat. Tech; 294 153-163.
22. K. Kulpetchdara, A. Limpichaipanit, G. Rujijanagul, Ch. Randorn, K. (2016). Chokethawai; "Influence of the nano-

hydroxyapatite powder on thermally sprayed HA coatings onto stainless steel"; Surf. Coat. Tech; 306 181-186.

23. B. Lin, M. Zhong, Ch. Zheng, L. Cao, D. Wang, L. Wang, J. Liang, B. (2015). Cao; "Preparation and characterization of dopamine-induced biomimetic hydroxyapatite coatings on the AZ31 magnesium alloy"; Surf. Coat. Tech; 281 82-88.
24. H. Li, Z. Guo, B. Xue, Y. Zhang, W. Huang. (2011). "Collagen modulating crystallization of apatite in a biomimetic gel system"; Ceram. Int.; 37 2305-2310.
25. C. Piccirillo, C.J. Denis, R.C. Pullar, R. Binions, I.P. Parkin, J.A. Darr, P.M.L. Castro; "Aerosol assisted chemical vapor deposition of hydroxyapatite-embedded titanium dioxide composite thin films"; J. Photochem. Photobiol; 332 (2017). 45-53.
26. G. Popescu-Pelin, F. Sima, L.E. Sima, C.N. Mihailescu, C. (2017). Luculescu, I. iordache, M. Socol, G. Socol, I.N. Mihailescu; "Hydroxyapatite thin films grown by pulsed laser deposition and matrix assisted pulsed laser evaporation: Comparative study"; App. Surf. Sci.; 418 580-588.
27. B.M. Hidalgo-Robatto, M. (2018). López-Álvarez, A.S. Azevedo, J. Dorado, J. Serra, N.F. Azevedo, P. González; "Pulsed laser deposition of copper and zinc doped hydroxyapatite coatings for biomedical applications"; Surf. Coat. Tech.; 333 168-177.
28. R. Schmidt, V. Hoffmann, A. Helth, P. (2016). Flaviu Gostin, M. Calin, J. Eckert, A. Gebert; "Electrochemical deposition of hydroxyapatite on beta-Ti-40Nb"; Surf. Coat. Tech.; 294 186-193.
29. D.H He, P. Wang, P. Liu, X.K. Liu, J. Zhao. (2016). "HA coating fabricated by electrochemical deposition on modified Ti6Al4V alloy"; Surf. Coat. Tech.; 301 6-12.
30. M. Farrokhi-Rad. (2017). "Electrophoretic deposition of hydroxyapatite fiber reinforced hydroxyapatite matrix nanocomposite coatings"; Surf. Coat. Tech.; 329 155-162.
31. R. M. Kumar, K. K. Kuntal, S. Singh, P. Gupta, B. Bhushan, P. (2016). Gopinath, D. Lahiri; "Electrophoretic deposition of hydroxyapatite coating on Mg–3Zn alloy for orthopedic application"; Surf. Coat. Tech.; 287 82-92.
32. R. Drevet, N. Ben Jaber, J. Fauré, A. Tara, A. B.Ch. Larbi, H. (2016). Benhayoune; "Electrophoretic deposition (EPD) of nano-hydroxyapatite coatings with improved mechanical properties on prosthetic Ti6Al4V substrates"; Surf. Coat. Tech.; 301 94-99.
33. S. Mahmoodi, L. Sorkhi, M. Farrokhi-Rad, T. (2013). Shahrabi; "Electrophoretic deposition of hydroxyapatite–chitosan nanocomposite coatings in different alcohols"; Surf. Coat. Tech.; 216 106-114.
34. H. Maleki-Ghaleh, V. (2012). Khalili, J. Khalil-Allafi, M. Javidi; "Hydroxyapatite coating on NiTi shape memory alloy by electrophoretic deposition process"; Surf. Coat. Tech.; 208 57-63.
35. M. Farrokhi-Rad, (2016). "Electrophoretic deposition of hydroxyapatite nanoparticles in different alcohols: Effect of Tris (tris(hydroxymethyl)aminomethane) as a dispersant", Ceram. Int., 42 3361-3371.
36. Shanaghi, Ali & Souri, Alireza & Chu, Paul &Mehrjou, Babak. (2024). Advanced Ceramics (Self-healing Ceramic Coatings).
37. M. Farrokhi-Rad, T. (2014). Shahrabi, "Effect of suspension medium on the electrophoretic deposition of hydroxyapatite nanoparticles and properties of obtained coatings", Ceram. Int., 403031-3039.
38. T.M. Sridhar, U.K. Mudali, and M. (2003). Subbaiyan, "Preparation and Characterization of EPD Hydroxyapatite Coatings on Type 316L SS", Corros. Sci., 45 237–252.
39. S. Kuche Loghmani, M. (2013). Farrokhi-Rad, T. Shahrabi, "Effect of polyethylene glycol on the electrophoretic deposition of hydroxyapatite nanoparticles in isopropanol", Ceram. Int., 39 7043-7051.
40. M. Farrokhi-Rad, T. Shahrabi. (2013). "Effect of triethanolamine on the electrophoretic deposition of hydroxyapatite nanoparticles in isopropanol", Ceram. Int., 39 7007-7013.
41. M. Wei, A.J. Ruys, B.K. Milthorpe, C.C. (2005). Sorrell, "Precipitation of hydroxyapatite nanoparticles: Effects of precipitation method on electrophoretic deposition", J. Mater. Sci.: Mater. Med. 16 [4] 319-324
42. X.F. Xiao, R.F. Liu. (2006). "Effect of suspension stability on electrophoretic deposition of hydroxyapatite coatings", Mater. Lett. 60 2627-2632.
43. J. Ma, C. Wang, K.W. Peng, (2003). "Electrophoretic deposition of porous hydroxyapatite scaffold", Biomaterials, 24 3505-3510.
44. M. Farrokhi-Rad, S. (2014). Loghmani, T. Shahrabi, Sh. Khanmohammadi, "Electrophoretic deposition of hydroxyapatite nanostructured coatings with controlled porosity", J. Eur. Ceram. Soc., 34 97-106.
45. J Cho, M. Cannio, A. R Boccaccini (2009). "The electrophoretic deposition of Bioglass®/carbon nanotube composite layers for bioactive coatings"; Int. J. Mater. Product. Tech.; 35 260- 270.
46. L. Besra and M. Liu. (2007). "A Review on Fundamental and Applications of Electrophoretic Deposition," Prog. Mater Sci., 52 1-61.
47. S.D. Cook, K.A. Thomas, J.E. Delton, T.K. (1992). Volkman, Th.S. Whitecloud, J.F. Key; "Hydroxylapatite coating of porous implants improve bone ingrowth and interface attachment strength"; J. Biomed. Mater. Res.; 26 989-1001.
48. H.Q. Nguyen, D.A. Deporter, R.M. Pilliar, N. (2004). Valiquette, R. Yakubovich; "The effect of sol–gel-formed calcium phosphate coatings on bone ingrowth and osteo conductivity of porous surfaced Ti alloy implants"; Biomaterials; 25 865-876.
49. H. Kienapfel, C. Sprey, A. (1999). Wilke, P. Griss; "Implant fixation by bone ingrowth", J. Arthroplasty.; 14 355-368.
50. P. Ducheyne, S. 1990). Radin, J.C. Heughebaert, M. Heughebaert; "Calcium phosphate ceramics coatings on porous titanium: effect of structure and composition on electrophoretic deposition, vacuum sintering and in vitro dissolution"; Biomaterials 11 (244-254.
51. H. Tang, T. Xin, F. Wang. (2013). "Calcium phosphate/titania sol-gel coatings on AZ31 magnesium alloy for biomedical applications"; Int. J. Electrochem. Sci.; 8 8115-8125.
52. F.X. Ye, A. Ohmori, T. Tsumura, K. Nakata, and C.J. Li. (2007). "Microstructural analysis and photocatalytic activity of

plasma-sprayed titania-hydroxyapatite coatings"; J. Therm. Spray Technol., 16 776-782
53. J. Y Han, Z T Yu, L Zhou. (2008). "Hydroxyapatite/titania composite bioactivity coating processed by the sol–gel method"; Biomed. Mater.; 3 044109.
54. H.W. Kim, H.E. Kim, V. (2005). Salih, J.C. Knowles; "Hydroxyapatite and titania sol–gel composite films on Ti; mechanical and in vitro biological performance"; J. Biomed. Mater. Res. 72 1–8.
55. M. Rothpan, N. Ch. T. Dadi, G. McKay, M. Tanzer, D. Nguyen, A. Hart, M. (2023). Tabrizian; "Titanium-dioxide-nanoparticle-embedded polyelectrolyte multilayer as an osteoconductive and antimicrobial surface coating"; Materials; 16 7026.
56. T Peltola, M Patsi, H. Rahiala. (1998). "Calcium phosphate induction by sol–gel-derived titania coatings on titanium substrates in vitro"; J. Biomed. Mater. Res. 41 504-510.
57. N. Watcharajittanont, M. Tabrizian, S. Ekarattanawong, J. Meesane; "Bone-mimicking scaffold based on silk fibroin incorporated with hydroxyapatite and titanium oxide as enhanced osteo-conductive material for bone tissue formation: fabrication, characterization, properties, and in vitro testing"; Biomed. Mater. 18 (2023) 65007.
58. H. Li, K. Khor, P. (2003). Cheang; "Impact formation and microstructure characterization of thermal sprayed hydroxyapatite/titania composite coatings"; Biomaterials; 24 949-957.
59. H. Farnoush, J. (2012). Aghazadeh Mohandesi, D. Haghshenas Fatmehsari, F. Moztarzadeh; "A kinetic study on the electrophoretic deposition of hydroxyapatite–titania nanocomposite based on a statistical approach"; Ceram. Int.; 38 6753–6767.
60. T. Kokubo, H. (2006). Takadama, how useful is SBF in predicting in vivo bone bioactivity? Biomaterials (15) 2907–2915.
61. L. Wang, J. Su, X. (2010). Nie, Corrosion and tribological properties and impact fatigue behaviors of TiN-and DLC-coated stainless steels in a simulated body fluid environment, Surf. Coat. Tech. 205 1599–1605.
62. Y. Lei, B. Song, R. D. (2017). Van Der Weijden, M. Saakes, and C. J. N. Buisman,"Electrochemical induced calcium phosphate precipitation: importance of localpH." Environ. Sci. Technol., 51, 11156
63. M. Amirnejad, M. Rajabi, and R. (2022). Jamaati, "Importance of individual evaluation of crystallographic texture and microstructure effects on biocompatibility and corrosion performance of Ti6Al4V alloy." Met. Mater. Int., 1
64. H. Benhayoune, R. Drevet, J. Fauré, S. Potiron, T. Gloriant, H. (2010). Oudadesse, andD. Laurent-Maquin, "Elaboration of monophasic and biphasic calcium phosphate coatings on Ti6Al4V substrate by pulsed electrodeposition current." Adv. Eng. Mater., 12, 192
65. E. Matykina, R. Arrabal, B. Mingo, M. (2016). Mohedano, A. Pardo, and M. C. Merino, "Invitro corrosion performance of PEO coated Ti and Ti6Al4V used for dental andorthopedic implants." Surf. Coatings Technol., 307, 1255
66. A. E. Nielsen. (1984). "Electrolyte crystal growth mechanisms." J. Cryst. Growth, 67, 289
67. D. Y. Lin and X. X. Wang. (2010). "Electrodeposition of hydroxyapatite coating onCoNiCrMo substrate in dilute solution." Surf. Coatings Technol., 204, 3205
68. A. Ito and K. Onuma, "Growth of hydroxyapatite Crystals." Crystal GrowthTechnology, ed. K. Byrappa, T. (2003). Ohashi, W. Michaeli, H Warlimont, and E. Weber (William Andrew Publishing, Norwich, NY) Ch 16, p 525–559
69. N. Horiuchi, K. Shibata, H. Saito, Y. Iwabuchi, N. Wada, K. Nozaki, K. Hashimoto, Y. Tanaka, A. Nagai, and K. (2018). Yamashita, "Size Control synthesis of hydroxyapatite plates and their application in the preparation of highly oriented films." Cryst. Growth Des., 18, 5038

DOI:10.31579/2767-7370/139